On the stability of magnetic paleodirection and paleointensity at microscale

Gelson F. Souza-Junior[1], Ualisson D. Bellon[2], Carolina S. de Moraes[1], Leonardo Uieda[1], Roger R. Fu[3], Wyn Williams[2], and Ricardo I. F. Trindade[1]

[1] Universidade de São Paulo, Brazil; [2] University of Edinburgh, UK; [3] Harvard University, USA;

Corresponding author: Gelson F. Souza-Junior <gelson.ferreira@iag.usp.br>

Received in original form on 2026/08/07.

Open research: The source code used to generate all of the results presented in this research can be freely accessed and reused under the terms of an open license. You can find it at https://doi.org/10.5281/zenodo.21841763 and https://github.com/compgeolab/micromag-paleoint.

Plain language summary

Rocks and archaeological materials preserve a record of Earth's ancient magnetic field as they cool. Traditionally, reconstructing this field has relied on bulk magnetic measurements. Using Quantum Diamond Microscopy, we show that stable estimates of both magnetic field direction and intensity can be obtained from hundreds to thousands of microscopic magnetic anomalies. We also demonstrate that individual magnetic anomalies can be thermally demagnetized, opening new possibilities for paleomagnetic and paleointensity investigations of heterogeneous, limited-volume, and high-value samples, including archaeological materials and meteorites.

Abstract

The geomagnetic field is a fundamental component of Earth's habitability, shielding the planet from high-energy cosmic radiation and solar-wind-driven atmospheric erosion. Understanding its long-term evolution relies on thermoremanent magnetization (TRM), the most robust recorder of past geomagnetic field direction and intensity. Traditionally, magnetic microscopy has been considered unsuitable for paleomagnetic reconstructions because classical statistical arguments suggested that millions of magnetic grains are required to overcome the stochastic nature of TRM acquisition and produce reliable estimates. However, recent micromagnetic modeling has challenged this view, predicting that the required population may be orders of magnitude smaller when vortex-state particles dominate the remanence. Here, we provide the first empirical validation of this prediction using Quantum Diamond Microscopy (QDM). We show that accurate paleodirectional information can be recovered from only hundreds to thousands of magnetic anomalies. We further demonstrate that absolute paleointensity can also be determined directly from QDM observations by combining high-resolution magnetic imaging with spatial filtering to isolate the most reliable magnetic sources within complex samples. Finally, we show that thermal Thellier–Thellier paleointensity experiments can be performed at the level of individual magnetic anomalies, minimizing multidomain bias while extending paleointensity analyses to heterogeneous geological materials, limited-volume specimens, and extraterrestrial materials.

1 Introduction

The geomagnetic field is a fundamental component of Earth's habitability, shielding the planet from high-energy cosmic radiation and solar wind-induced atmospheric erosion. Significant reductions in field intensity throughout geological time are thought to increase the flux of energetic particles reaching the surface, potentially driving environmental shifts (Bono et al., 2019). For instance, unusually low field strengths during the Ediacaran-Cambrian transition have been proposed as a contributing factor to the environmental pressures surrounding the Cambrian diversification (Huang et al., 2024). Thus, quantifying the absolute intensity of the paleo-field is essential for reconstructing geodynamo evolution and its broader interactions with the Earth system.

The reliability of paleomagnetic records ultimately depends on the stability of the magnetic carriers responsible for preserving the ancient geomagnetic field. Thermoremanent magnetization (TRM) remains the most robust recorder of past field direction and intensity and forms the theoretical basis of classical paleointensity methods (Néel, 1949; Thellier and Thellier, 1959). During cooling through the Curie temperature in the presence of an external magnetic field, magnetic moments progressively lock into energetically favorable states as thermal fluctuations decrease. TRM acquisition can therefore be understood as a statistical process in which a population of magnetic grains collectively samples the ambient magnetic field.

However, stable recording is restricted to a relatively narrow range of grain sizes and magnetic configurations. Single-domain (SD) grains exhibit uniform magnetization and strong magnetic stability, making them ideal TRM recorders. With increasing grain size, magnetic structures evolve into more complex states such as single-vortex (SV), multi-vortex, and ultimately multi-domain (MD) configurations (Nagy et al., 2019). The domain wall motion within the MD grains can significantly reduce magnetic stability (Dunlop and Özdemir, 1997). Consequently, paleodirectional estimates are generally more reproducible than paleointensity determinations, which are particularly sensitive to unstable or interacting grains.

The statistical requirements for reliable paleointensity estimates from TRM have long been debated. Based on the original theory for single-domain grains, it has been suggested that very large populations of grains are required to accurately record the geomagnetic field. For instance, Berndt et al. (2016) argued that millions of SD grains may be necessary to obtain precise directional and intensity estimates at Earth's field strengths due to the relatively low efficiency of TRM acquisition ($\leq$ 1%, Kletetschka et al., 2004). However, this estimate is based on the assumption that TRM recording is dominated by ideal SD particles. Increasing evidence indicates that larger grains in vortex states are widespread in natural samples and often represent the main carriers of remanence (Gergov et al., 2025). Recent micromagnetic modeling considering a population of single-vortex grains shows that hundreds to thousands of grains are sufficient to provide the statistical requirement for the reliable recording of the ambient field (Bellon et al., 2025).

Recent advances in magnetic microscopy and quantitative imaging offer new opportunities to isolate individual magnetic sources and distinguish stable recorders from unstable particles within complex natural assemblages (Fu et al., 2020; Glenn et al., 2017). In this study we explore this possibility using high-resolution magnetic imaging combined with dipolar inversion techniques. Paleodirectional and paleointensity experiments were conducted on two samples with contrasting magnetic behavior: a ceramic fragment dominated by SD and SV grains, and a basalt containing a significant fraction of MD carriers. The ceramic sample provides a near-ideal TRM recorder, whereas the basalt represents a magnetically more complex system dominated by larger grains and multidomain behavior. By comparing these contrasting materials, we evaluate how micro-scale magnetic analysis can identify stable magnetic carriers and improve the reliability of paleointensity determinations.

2 Methodology

All experiments and magnetic measurements were conducted at the Harvard Paleomagnetics Laboratory, Department of Earth and Planetary Sciences, Harvard University. The laboratory facilities are magnetically shielded to minimize interference from the ambient geomagnetic field and external magnetic noise. This environment ensures that remanent magnetizations acquired during the experiments are controlled solely by the applied laboratory fields and that magnetic measurements are not affected by external field variations. These experimental conditions were maintained consistently throughout all heating, cooling, and measurement steps.

2.1 Sample Selection and Preparation

Two materials with contrasting magnetic characteristics were selected to evaluate the performance of QDM-based paleointensity analysis. The first sample consists of a fragment of baked archaeological ceramic (RSLG1) from the São Luiz Gonzaga Jesuit reduction (1657–1687 AD). Previous magnetic characterization by Poletti et al. (2016) indicates that its remanent magnetization is primarily carried by low-coercivity, Ti-poor titanomagnetite with pseudo-single-domain (PSD) to single-domain (SD) behavior, exhibiting saturation fields below 0.3 T and demagnetization temperatures approaching 550 °C. Such properties make this material a suitable reference case for testing the method under relatively stable and weakly interacting magnetic conditions.

To contrast with this relatively well-behaved system, a basalt from the Caviahue–Copahue volcanic complex (Argentina) was selected. This sample, originating from the Cola de Zorro Formation, represents a more magnetically complex natural system. Its magnetic mineralogy is dominated by low-Ti magnetite distributed within a trachytic volcanic matrix containing phenocrysts and finer-grained phases. Rock magnetic experiments reported for this formation indicate generally low coercivities and saturation fields around 0.2 T, with domain states ranging from pseudo-single-domain to multidomain behavior depending on grain size and local mineralogical variations (Moncinhatto et al., 2019).

Both samples were prepared as polished small chips suitable for quantum diamond microscopy and bulk measurements. This preparation ensures a flat, stable surface, minimizing sensor-to-sample distance and enabling high-resolution magnetic field mapping.

2.2 TRM Acquisition

Thermoremanent magnetizations (TRMs) were induced by heating the samples in an induction furnace to a maximum temperature of 700 °C, where they were held for 30 minutes to ensure complete thermal demagnetization. The samples were then cooled slowly under a controlled laboratory magnetic field applied along a horizontal direction (Dec = 0°, Inc = 0°). The cooling occurred naturally over approximately 8 hours until room temperature ($\sim 25\ ^\circ$C) was reached, with the bias field applied continuously throughout the cooling process.

Successive TRMs were induced in the same sample using laboratory fields of 2, 10, 50, and 100 μT to evaluate the efficiency of TRM acquisition under different field intensities. The 50 μT TRM was induced last, as this field corresponds to the bias field used in the subsequent paleointensity experiments.

Following the TRM acquisition, remanence measurements were performed using a 2G Enterprises superconducting rock magnetometer. In addition, ten fields of view (FoVs) were imaged with the QDM for each induced TRM to characterize the spatial distribution of the magnetic sources. The induced TRMs were subsequently demagnetized using alternating fields (AF) up to 100 mT, and the primary magnetization component was isolated using principal component analysis (PCA, Kirschvink, 1980). The only exception was the TRM induced under the 50 μT laboratory field, for which demagnetization was performed thermally as part of the subsequent paleointensity experiment.

2.3 Paleointensity Experiments

Absolute paleointensity experiments were performed using a Thellier–Thellier double-heating ZI (Zero field - In field, Coe, 1967) protocol applied to the samples carrying the synthetic TRM induced under a laboratory field of 50 μT. Natural remanent magnetization (NRM) was progressively demagnetized through stepwise heating at 100, 200, 300, 400, 500, and 600 °C. A pTRM check was performed by repeating the 500–300 °C step to monitor possible mineralogical alteration during the experiment.

To minimize potential anisotropy effects, the laboratory field applied during the in-field heating steps was parallel to the direction used to induce the synthetic TRM and had the same intensity (50 μT). Because the cooling rate during TRM acquisition and during the paleointensity steps was identical, no cooling-rate correction was applied.

The ancient field intensity (H_{anc}) was estimated from the ratio between the remaining NRM and the acquired pTRM during each temperature step according to

$$H_{anc} = \left| \frac{\mathrm{NRM}_{\mathrm{remaining}}}{\mathrm{pTRM}_{\mathrm{acquired}}} \right| H_{lab}, \tag{1}$$

where $\mathrm{NRM}_{\mathrm{remaining}}$ is the remaining natural remanent magnetization after each demagnetization step, $\mathrm{pTRM}_{\mathrm{acquired}}$ is the partial thermoremanent magnetization gained during the corresponding in-field step, and H_{lab} is the laboratory field intensity.

All remanence measurements were performed using a 2G Enterprises superconducting rock magnetometer. In addition, five FoVs were imaged with the QDM at each experimental step to monitor the evolution of individual magnetic sources during the paleointensity experiment.

2.4 QDM Magnetic Inversion and Data Processing

Surface magnetic flux density maps were acquired using a Quantum Diamond Microscope (QDM) at each temperature step, with stray fields measured at an estimated distance of $\sim 5\ \mu$m from the sample surface. The LED-based registration algorithm of Bellon et al. (2026a) was used to align all FoVs acquired throughout the experiment. The magnetic moments of individual anomalies were extracted using the spherical harmonic inversion approach of Souza-Junior et al. (2026b), in which the magnetic field is represented by a spherical harmonic expansion up to third degree, centered on the Euler deconvolution solution. The Euler solution itself was determined following the methodology of Souza-Junior et al. (2025). We evaluated a range of model-fitting criteria ($R^2 \geq 0.90$ to 0.98) to investigate how the quality of the magnetic source inversion influences the recovered TRM directions and paleointensity estimates. For each R^2 threshold, only anomalies satisfying the corresponding model-fitting criterion were retained. Population-level TRM directions and Fisher directional statistics (Fisher et al., 1987) were calculated using the *PmagPy* software package (Tauxe et al., 2016) from anomalies with $R^2 \geq 0.95$. In contrast, paleointensity estimates were evaluated across the full range of R^2 thresholds.

For the paleointensity analysis, the remaining NRM and acquired pTRM were calculated at each thermal step for each retained anomaly, enabling the construction of individual anomaly-scale Arai plots. For each R^2 threshold, paleointensity estimates from all accepted anomalies were averaged to obtain the recovered field and its associated uncertainty, while the number of contributing anomalies was tracked. This procedure allowed us to quantify the trade-off between inversion quality, the size of the anomaly population, and the accuracy and precision of the recovered paleointensity estimates.

3 Results

3.1 Statistical Efficiency and Directional Convergence

The analysis of TRM acquisition across varying bias field strengths (2, 10, 50, and 100 μT) reveals a clear relationship between field intensity and directional stability at the microscopic scale. As the bias field strength increases, the alignment of individual magnetic anomalies becomes progressively more coherent, as evidenced by the decreasing dispersion in the stereographic projections (Figure 1).

Fisher statistics (Fisher et al., 1987) calculated from the complete population of magnetic anomalies are summarized in Table 1. For both basalt and ceramic samples, the confidence cone (α_{95}) systematically decreased with increasing field intensity and resultant vector length, reaching values as low as 2.80° despite the broad directional dispersion of the anomalies, as shown by their high circular standard deviations (CSD) values (between 64.5° and 80.5°) for several analyzed anomalies varying between 3714 and 5253). The Fisher precision parameter (k) remained low across all applied field intensities, ranging from 1.013 to 1.575. However, as shown in Figure 2, both parameters exhibit an approximately linear dependence on the applied bias field. The Fisher precision parameter (k) increases linearly with field intensity, whereas CSD decreases.

Table 1: Fisher statistics for individual anomalies under different field intensities.

Sample	Field (μT)	N	R	k	α_{95} (°)	CSD (°)
Basalt	2	5095	278.1	1.058	8.19	78.8
	10	5253	354.1	1.072	7.20	78.2
	50	4835	1194.5	1.328	3.52	70.3
	100	4502	1610.4	1.557	2.80	64.9
Ceramic	2	4839	63.9	1.013	17.50	80.5
	10	4303	316.5	1.079	7.60	78.0
	50	4316	1047.4	1.320	3.77	70.5
	100	3714	1357.0	1.575	3.03	64.5

At very low field strengths (2 μT), individual anomalies exhibit a high degree of stochastic scatter and the lowest values for k, reflecting the limited ability of alignment of the grain's magnetic moment to the field direction. However, for all bias fields above 2 μT, both the recovered Fisher mean and vector sum directions from the QDM measurements coincide well with the bulk directions obtained from Superconducting Quantum Interference Device (SQUID) measurements. This consistency suggests that the signal from a discrete population of magnetic anomalies effectively represents the sample's macroscopic remanence.

The number of detected anomalies (N) required to achieve a statistically reliable direction (defined here as an angular misfit ≤ 5°; gray area in Figure 1) depends strongly on the bias field intensity. For stronger fields (≥ 50 μT), a few hundred anomalies are sufficient to reach this threshold in both basaltic and ceramic samples, although k is never greater than 2. For lower fields, such as 10 μT, the required

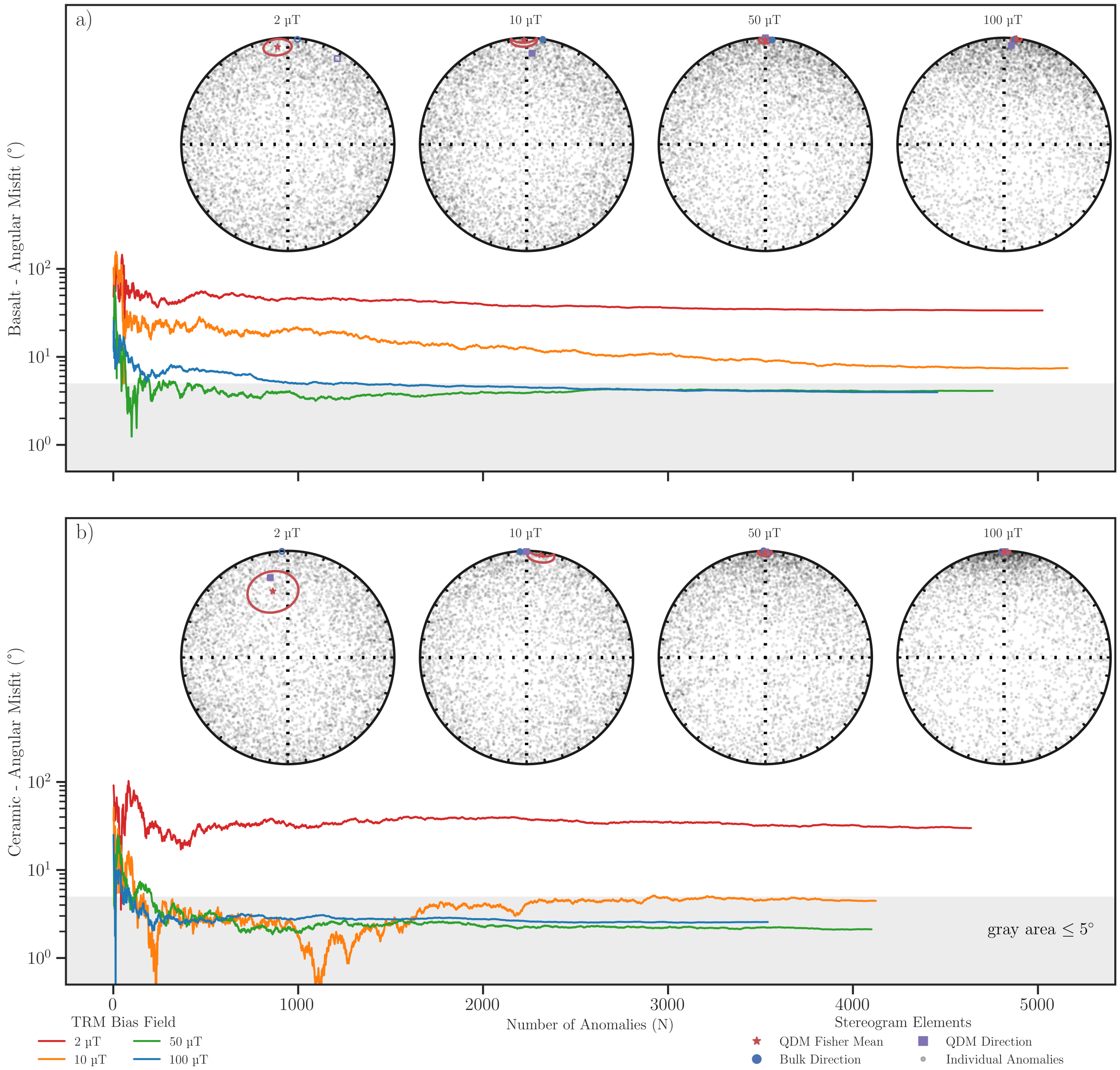

Figure 1: Statistical efficiency and directional convergence of magnetic microscopy. High-resolution directional analysis proves that accurate remanence orientations can be retrieved from limited analytical volumes. The main panels show the angular misfit relative to the bulk measurements as a function of the number of detected anomalies (N) for basalt (top) and ceramic (bottom). In the gray area, the directional error falls below the 5° threshold. Insets provide stereographic projections of individual anomaly directions (gray circles), the total vector sum of these directions (purple squares), Fisher mean directions (red stars), and lastly the bulk direction (blue circles) across field strengths of 2, 10, 50, and 100 μT, highlighting the increased grouping at higher intensities.

population size increases to several hundred for the ceramic sample and up to a few thousand for the more complex basaltic rock (Figure 1), although the latter stabilizes at a misfit of around 8°. These results provide empirical confirmation of recent micromagnetic models suggesting that the particle count needed for reliable paleomagnetic estimates is significantly lower than previously estimated, particularly when considering carriers in the single-vortex state.

The efficiency of anomaly detection decreases significantly as the bias field increases. This trend suggests that as the external field strength intensifies, the individual magnetic moments become not only stronger but also more ideally dipolar, effectively increasing the signal-to-noise ratio for the most efficient carriers. Consequently, these dominant, high-intensity sources tend to mask the signals from weaker or less stable neighboring grains, resulting in a smaller but more robust population

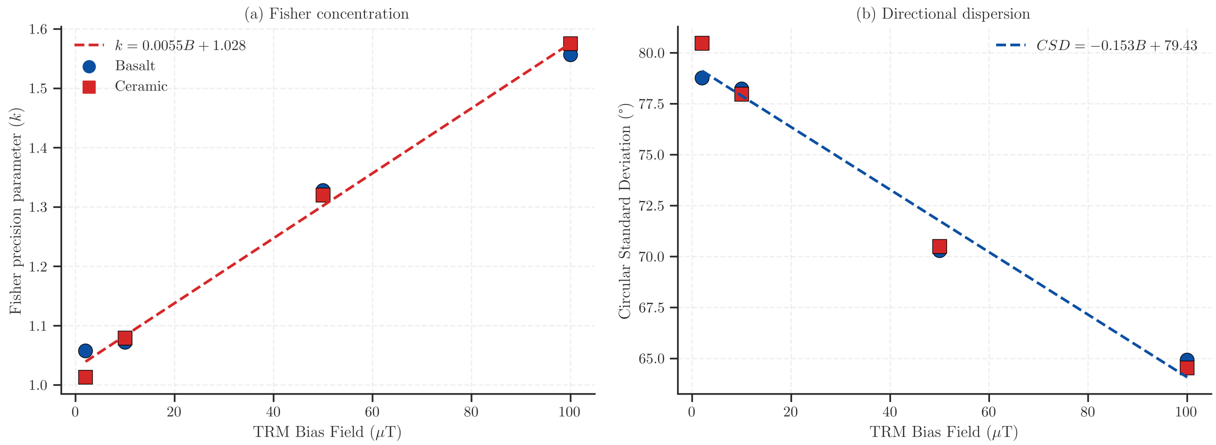

Figure 2: Fisher directional statistics calculated from the QDM-derived magnetic moment vectors as a function of the applied TRM bias field. (a) Fisher precision parameter (k) and (b) circular standard deviation (CSD) for the basalt (blue circles) and ceramic (red squares) samples. Dashed lines represent linear least-squares fits to the combined dataset.

of anomalies that meet the strict dipolarity filtering criterion. This “masking effect" at higher fields further explains the rapid directional convergence observed, as the resulting population is inherently biased toward the most reliable magnetic recorders in the matrix.

3.2 Bulk Paleointensity Measurements

The conventional Thellier-Thellier bulk measurements (Figure 3) provided a primary benchmark for evaluating the accuracy of the magnetic microscopy approach against the 50 μT laboratory bias field. For both samples, the recovered paleointensities reached values close to the applied field, although they did not perfectly overlap even when considering analytical uncertainties. The basaltic sample yielded a bulk value of $B_{anc} = 52.6 \pm 1.356$ μT (Figure 3b), while the ceramic sample resulted in $B_{anc} = 46.2 \pm 0.358$ μT (Figure 3e).

A notable feature in the basaltic sample is the incomplete thermal demagnetization at 600°C (Figure 3a). This indicates the presence of minerals with high blocking temperatures, likely hematite, potentially formed during laboratory heating. Since the 50 μT TRM acquisition step was the final procedure performed on these specimens, cumulative thermal alteration is a likely factor. While the ceramic sample also exhibits traces of high-temperature remanence, it undergoes nearly complete demagnetization, suggesting that the magnetic signal remains dominated by magnetite, which effectively masks any minor hematite contribution (Figure 3d). Despite these mineralogical complexities, the characteristic remanent magnetization (ChRM) directions for both materials remain highly consistent with the known orientation of the laboratory bias field (Figure 3c, f).

The Arai plot for the basaltic specimen displays a slight downward curvature (Figure 3b). Given that the pTRM checks remained successful, indicating a lack of significant mineralogical alteration affecting the capacity to acquire remanence. Therefore, this "bulging" behavior is interpreted as a signature of the presence of a population of MD magnetite grains within the basaltic matrix and can be detrimental to paleointensity estimates (Dunlop et al., 2005).

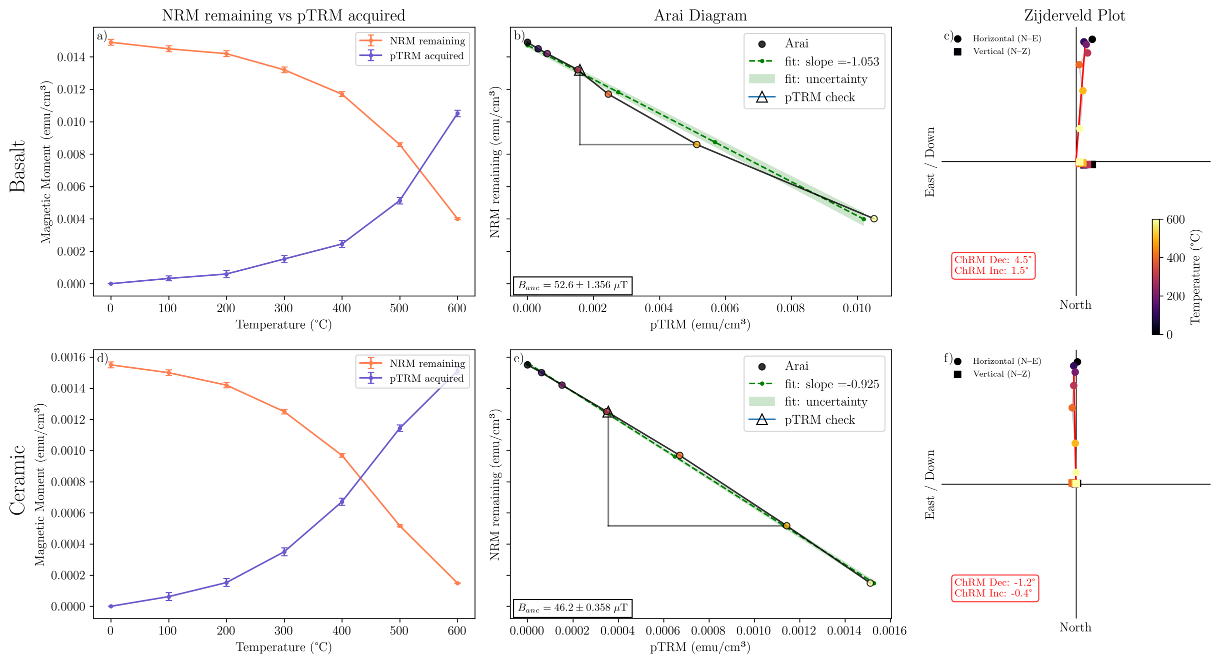

Figure 3: Bulk paleointensity benchmark and directional stability. (a, d) Magnetic moment remaining (NRM) and pTRM acquired as a function of temperature for basalt and ceramic specimens. (b, e) Arai diagrams showing the linear regression fit (dashed green line) and associated uncertainty (shaded green area) for the absolute paleointensity estimates. Open triangles indicate pTRM checks from 500°C to 300°C. (c, f) Zijderveld plots displaying the horizontal (circles) and vertical (squares) components of the remanent magnetization vector, with characteristic remanent magnetization (ChRM) direction in red.

3.3 QDM Absolute Paleointensity: From Population Averages to Single-Anomaly Resolution

The application of iterative multipolar inversion to QDM magnetic maps allows for a multi-scale validation of absolute paleointensity. By transitioning from automated population-level averages to the analysis of individual high-quality carriers, we demonstrate the robustness of the microscopy approach in recovering the 50 μT laboratory bias field.

As shown in Figure 4, the paleointensity estimates derived from the anomaly population exhibit a clear convergence as the filtering criterion are refined. For the more complex basaltic sample, the population-level intensity and its associated uncertainty vary over the fitting model threshold range from 0.90 to 0.98 (Figure 4a); however, its mean behavior (B_{anc} = 48.4 ± 2.2 μT) encompasses the true bias field intensity. On the other hand, the ceramic sample showed statistically the same range of results for all steps of filtering. In contrast, the ceramic sample shows remarkable stability across all filtering levels, yielding a consistent mean of B_{anc} = 50.8 ± 0.9 μT. The reliability of these population-level estimates is supported by positive pTRM-checks (Figure 5b, e), which fall directly on the expected value or the primary linear segments of the Arai plots, indicating no significant thermal alteration during the experiment. Both samples exhibit ideal univectorial decay toward the expected laboratory direction as shown by the Zijderveld diagrams (Figure 5c, f), especially after 300°. Hence, the latter was used as the cut-off for the Arai diagram fitting.

Figure 6 shows the behavior of an individual magnetic anomaly, likely representing a small cluster or magnetic minerals, during a double-heating paleointensity experiment. The paleointensity estimate obtained from the vector summation of the magnetic moment of this anomaly yielded 50.8 ± 1.41 μT, closely matching the imposed 50 μT bias field. The corresponding Arai relationship was constructed from the thermal evolution of the magnetic moment, and the anomaly also passed the pTRM-check, indicating stable remanence acquisition during the experiment. These results demonstrate that individual anomalies identified at the grain scale can preserve reliable thermal remanence behavior and provide accurate paleointensity estimates. A comparable single-anomaly characterization was not possible for the basalt sample, where the magnetic sources exhibited more complex behavior and did not yield isolated carriers with a similarly well-defined thermal response.

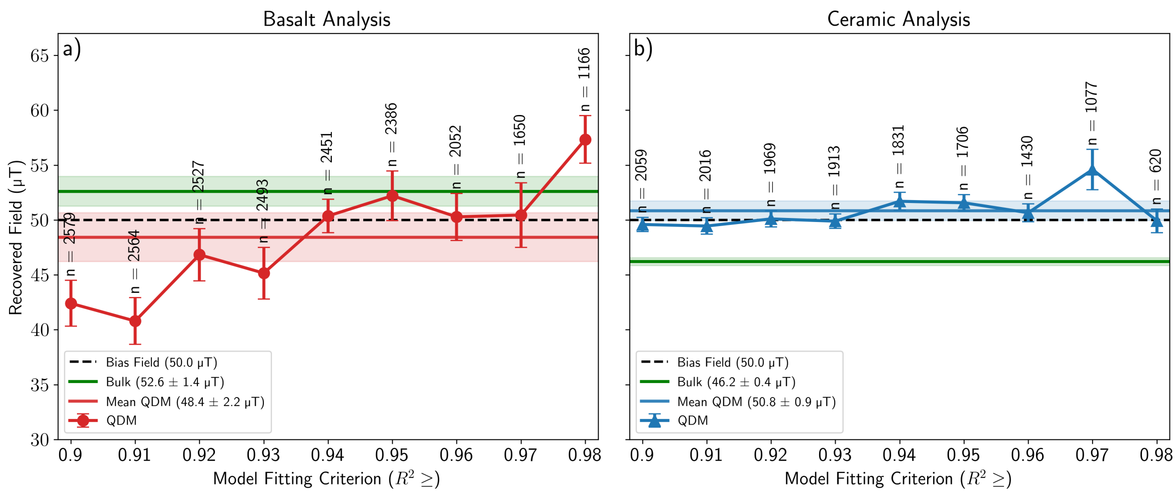

Figure 4: Paleointensity estimates from QDM data under varying goodness-of-fit filtering criterion for (a) basalt and (b) ceramic samples. The dashed black line indicates the laboratory bias field (50 μT). Green lines and shaded bands represent the bulk Thellier–Thellier paleointensity estimates and their respective uncertainties. Each curve shows the mean paleointensity obtained from QDM-filtered anomaly populations as a function of progressively stricter goodness-of-fit thresholds. Error bars represent one standard deviation of the selected anomaly population.

4 Discussion

4.1 Reevaluating Statistical Limits in Microscopic Paleomagnetism

A long-standing paradigm in paleomagnetism, as proposed by Berndt et al. (2016), suggested that millions of stable magnetic carriers were required to statistically average out the stochastic nature of magnetization and obtain a reliable field estimate. Our empirical findings directly challenge this statistical limit. Instead, the QDM observations provide empirical validation for the recent micromagnetic models by Bellon et al., (Bellon et al., 2025), even though anomalies identified by the QDM can arguably be interpreted as a cluster of grains for the QDM settings (Bellon et al., 2026b). This demonstrates that a significantly smaller population of grains can reliably record the ambient magnetic field.

The observed relationship between bias field strength and the number of required anomalies (N) perfectly mirrors the numerical predictions for single-vortex (SV) particle assemblages. Bellon et al. (2025) modeled that for external fields ≥ 10 μT, a few thousand nanoscopic vortex-state particles are sufficient to record a TRM with an angular misfit of less than 1°. Our empirical data confirms this threshold: at a 10 μT field, we found that reaching a stable direction (misfit ≤ 5°) requires hundreds to a few thousand anomalies, depending on the sample's complexity. Furthermore, for stronger fields (≥ 50 μT), our observation that only a few hundred anomalies are needed aligns with the models showing that even small assemblages of SV particles can rapidly minimize directional uncertainty under Earth-like field intensities. Conversely, the high stochastic scatter we recorded at 2 μT corroborates the theoretical lower limit proposed (Bellon et al., 2025), which demonstrated that very weak fields ($< 2\ \mu$T) fail to produce a reliable net magnetization. Nevertheless, the bulk measurement still provides a reliable direction for the weaker bias field. This is expected because the bulk measurements reflect a larger volume, and thus sample a larger number of stable magnetic grains, than the magnetic microscopy images.

The fundamental discrepancy between our empirical reconstructions and the estimates of Berndt et al. (2016) stems from two key physical and methodological differences, as recently elucidated by Bellon et al. (2025). First, the previous models assumed idealized SD particles characterized by uniaxial anisotropy. However, magnetic minerals in natural igneous rocks predominantly exist in a pseudo-single-domain (PSD) state, characterized by vortex structures (Gergov et al., 2025). These vortex-state particles exhibit multiaxial anisotropies (e.g., spherical and oblate shapes possessing multiple easy axes of magnetization), which significantly increases the statistical probability that a particle's magnetic moment will align favorably with the external field. This multiaxial nature drastically enhances TRM acquisition efficiency, requiring far fewer grains to achieve a coherent macroscopic remanence.

Second, the statistical framework traditionally employed in paleomagnetic studies, such as that adopted by Berndt et al. (2016), relies on population-based confidence parameters (e.g., α_{95}) to evaluate directional fidelity. This approach inherently assumes that the dispersion of individual observations is the primary measure of recording quality. However, this assumption becomes problematic when applied to microscale magnetic datasets. In the present study, as in the numerical models of Bellon et al. (2025), directional accuracy is evaluated instead using angular misfit. This distinction is particularly important because the combination of low Fisher precision parameters ($k \leq 2$), exceptionally large circular standard deviations (up to 80.5°), and relatively small confidence cones highlights a fundamental limitation of conventional Fisher statistics at the particle scale. The latter due to a high value for N.

Unlike bulk paleomagnetic measurements, where each specimen represents an averaged magnetic signal, microscale analyses treat thousands of individual magnetic anomalies as independent observations, naturally capturing the intrinsic stochasticity of remanence acquisition arising from grain geometry, magnetostatic interactions, and non-ideal recording behavior. As a consequence, the very large number of observations artificially constrains α_{95} to deceptively small values. However, the underlying population remains physically highly dispersed as shown by the k values for both samples at different bias fields, which reflects the low efficiency in the TRM acquisition. Therefore, small confidence cones should not be interpreted as evidence of uniformly reliable magnetic recorders in microscale paleomagnetic experiments.

While the numerical models of Bellon et al. (2025) focused primarily on SV ellipsoids, our empirical observations on basaltic and ceramic samples likely encompass a broader range of domain states (*e.g.*, Out et al., 2024), including MV particles typically found in irregular natural grains. The fact that our natural samples acquired a coherent TRM with relatively few particles supports the theoretical proposition that complex, irregular grain shapes exhibit local energy minima that act as multiple easy axes. This multiaxial behavior in vortex-state grains facilitates efficient alignment with the applied field, much like the oblate and spherical SV particles (Bellon et al., 2025). The slight discrepancy we observed at 10 μT, where the more complex basaltic rock required a larger population size compared to the ceramic sample, may reflect the broader diversity of grain morphologies and the presence of these more complex multi-vortex structures in the natural igneous matrix.

Ultimately, our QDM measurements provide the critical observational evidence needed to support these recent micromagnetic models, confirming that paleomagnetic analyses on microscopic samples, single crystals, and highly valuable extraterrestrial materials are statistically sound and physically reliable, provided the ancient magnetic field was sufficiently strong ($\geq 2 - 10\ \mu$T).

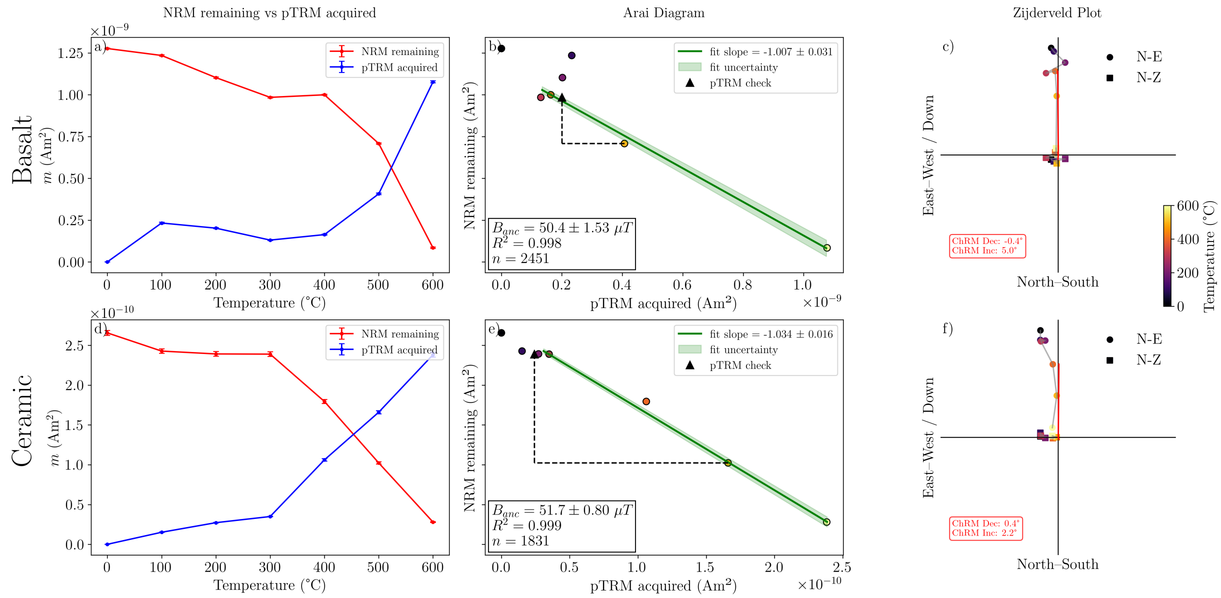

Figure 5: Representative Thellier–Thellier paleointensity results obtained from QDM-derived magnetic anomalies for the basalt (top row) and ceramic (bottom row) samples after applying a filtering criterion. (a,d) NRM remaining (orange) and pTRM acquired (blue) as a function of temperature, showing the progressive replacement of the natural remanent magnetization during the heating steps. (b,e) Corresponding Arai diagrams with linear fits (green dashed line) used to estimate the paleointensity; the shaded region indicates the uncertainty of the fit, and the triangle marks the pTRM check. (c,f) Zijderveld diagrams illustrating the thermal demagnetization behavior of the same anomalies, with circles representing the horizontal projection (N–E) and squares the vertical projection (N–Z); colors indicate temperature steps.

4.2 Implications for Absolute Paleointensity from Magnetic Microscopy

The convergence of our empirical data with recent micromagnetic models strongly endorses the expanding use of magnetic microscopy techniques, such as the QDM and SQUID microscopy (Fu et al., 2020; Glenn et al., 2017; Weiss et al., 2007). Therefore, it is possible to extract reliable paleointensity with only a few hundred dipolar anomalies. The capability of magnetic microscopy to selectively filter dipolar sources offers a robust solution to the pervasive issue of multi-domain (MD) bias in absolute paleointensity studies. In the basaltic sample, the bulk Arai plot exhibited a downward “bulge” characteristic of non-ideal MD behavior, which typically leads to systematic intensity errors in conventional bulk measurements. By acting as a high-resolution “filter” through a strict goodness-of-fitting criterion, the QDM effectively isolated ideal magnetic recorders from the complex volcanic matrix. This selective integration surgically removes the non-linear MD noise, demonstrating that microscopy can be used as a method for paleointensity estimates from mineralogically complex samples.

However, the basalt experiment reveals that dipolarity alone is not a sufficient condition for ideal paleointensity behavior. Although the application of strict criterion successfully isolates anomalies that are geometrically consistent with “well-behaved” magnetic sources, none of the basaltic anomalies produced linear individual Arai plots. This observation suggests that additional physical processes may remain unresolved even after removing magnetic contributions greater than the third degree of the spherical harmonic expansion. A first possibility is the presence of strongly interacting single-domain assemblages, where magnetostatic interactions between neighboring grains perturb the independence of TRM acquisition (*e.g.,* Carvallo et al., 2006). A second possibility relates to the experimental protocol itself, as several anomalies systematically exhibit enhanced demagnetization between 500 and 600°C, indicating that the selected temperature intervals may not optimally resolve critical unblocking temperature spectra. In addition, the absence of pTRM-tail checks prevented a direct assessment of the multidomain-related non-ideal behavior. These observations demonstrate that while filtering represents a major step toward eliminating multidomain-related bias, additional anomaly-scale selection criterion remain necessary to fully identify ideal paleointensity recorders.

Although recent studies have demonstrated that magnetic microscopy can recover paleointensity information at the microscale, these efforts have so far been limited to non-thermal protocols. For example, Bellon et al. (2026a) successfully applied a pseudo-Thellier method to the same archaeological ceramics, successfully estimating paleointensity from individual magnetic carriers identified by QDM. However, this approach intrinsically depends on empirical calibration factors, which, although useful for easily altered materials, limit its application as a direct paleointensity method. Here, we demonstrate that QDM can instead be combined with a classical thermal Thellier-Thellier protocol, allowing paleointensity to be determined directly by targeting the blocking-temperature spectrum. This represents an important step toward absolute microscale paleointensity measurements that remain fully consistent with the physical basis of conventional thermal paleointensity experiments.

Furthermore, the transition to single-anomaly resolution establishes a new benchmark for experimental precision. The fact that isolated dipolar sources can accurately recover the laboratory bias field proves that the fundamental physics of TRM is preserved at the single-crystal level. Crucially, this grain-specific approach allows for the implementation of pTRM checks on individual anomalies throughout the heating process. By monitoring the occurrence of thermal alterations at the scale of single anomalies, it becomes possible to identify and exclude compromised carriers while retaining those that remain stable. This selective methodology significantly enhances the success rates of paleointensity experiments, as high-fidelity geophysical information can be retrieved even when only a small fraction of the sample volume remains unaltered.

Finally, the systematic relationship between the TRM acquisition field and the directional statistics of the recovered anomaly population suggests an intriguing alternative to conventional laboratory paleointensity experiments. Both the Fisher concentration parameter and the circular standard deviation exhibit approximately linear trends with increasing TRM bias field (Figure 2), indicating that stronger magnetic fields produce progressively better alignment among individual magnetic carriers. This behavior reflects the increasing ability of the ambient magnetic field to overcome thermal fluctuations during TRM acquisition, producing a more tightly clustered distribution of remanence directions. Remarkably, both the basalt and ceramic samples follow the same first-order trend despite their contrasting lithologies and magnetic behaviors, suggesting that these statistical parameters are primarily controlled by the intensity of the applied field rather than by sample-specific characteristics.

This observation raises the possibility of estimating paleofield intensity directly from the directional statistics of magnetic microscopy datasets, without requiring laboratory heating experiments or repeated TRM acquisition. Rather than reconstructing the original magnetization through Thellier-type protocols, the paleofield would be inferred from the degree of directional ordering preserved within the natural remanence itself. Conceptually, this approach is analogous to paleointensity methods developed for depositional remanent magnetization (DRM), in which the strength of the ambient magnetic field is inferred from its ability to align magnetic particles during sediment deposition (Ostermeier et al., 2026). Here, the same physical principle is applied to thermoremanent magnetization: stronger magnetic fields produce more coherent grain-scale remanence directions, leaving a measurable statistical signature that can be quantified through Fisher parameters.

Although this concept requires calibration across a broader range of magnetic field intensities, mineralogies, grain-size distributions, and geological materials, the present results provide the first experimental evidence that directional statistics derived from magnetic microscopy may contain quantitative paleointensity information. If validated, this approach could establish a fundamentally new paleointensity proxy capable of extracting field intensity directly from magnetic images, substantially reducing the need for destructive laboratory heating experiments while greatly expanding the range of materials suitable for absolute paleointensity investigations.

4.3 Applications to Extraterrestrial Materials and Weak-Field Environments

Our empirical validation of efficient TRM acquisition in small grain assemblies has profound implications for the paleomagnetic analysis of high-value and extraterrestrial materials, particularly for the study of meteorites and samples returned from space missions, including the Moon (Cai et al., 2025; Nichols et al., 2021), Mars (Jung et al., 2024; Weiss et al., 2025), or asteroids (Bates, 2026). In these contexts, material is extremely scarce, and conventional bulk methods are often unfeasible due to mass requirements or the risk of destroying unique specimens. Our results show that accurate absolute paleointensity can be recovered from a manageable number of grains within a sub-millimeter area. This opens a robust pathway for decoding the magnetic history of the early sufficient-to-estimate fragments, where the ability to isolate primary remanence from background noise or secondary alterations is critical. Our findings confirm that researchers can confidently employ micro-sampling and non-destructive magnetic microscopy on these invaluable specimens. As long as the planetary dynamo produced a field strength $\geq 10\ \mu$T, sub-sampling strategies will not compromise the statistical reliability of the extracted paleomagnetic data.

Conversely, the stochastic scatter we observed at $2\ \mu$T serves as a critical empirical limit. This observation aligns with micromagnetic predictions that weak fields ($< 2\ \mu$T) fail to impart a stable, uniform remanence across small grain populations. This physical limitation must be carefully considered when investigating periods of hyperactive geomagnetic reversals or near-collapse of the geodynamo, such as the Late Ediacaran period, or when analyzing certain meteoritic samples (Bryson et al., 2020; Levashova et al., 2021).

Because the QDM approach targets stable signals from individual magnetic grains, it performs particularly well in ceramic materials and may enable the recovery of reliable paleointensity estimates from samples that previously failed conventional experiments. Such measurements would help constrain the magnitude and evolution of the South Atlantic Magnetic Anomaly (SAMA) through time. Beyond deep-time scenarios and extraterrestrial materials, this technique may also provide a valuable alternative for revisiting paleointensity measurements from pre-Columbian ceramics in South America, which are abundant but often unsuitable for traditional methods due to incomplete baking. This limitation has contributed to a severe scarcity of absolute intensity data in the Southern Hemisphere, with South America representing less than 3% of the global geomagnetic database (Trindade et al., 2018).

Data, Materials, and Software Availability

The Python code used to generate all results and figures presented in this study, as well as the QDM magnetic microscopy data analyzed here, are available through Souza-Junior et al. (2026a). These

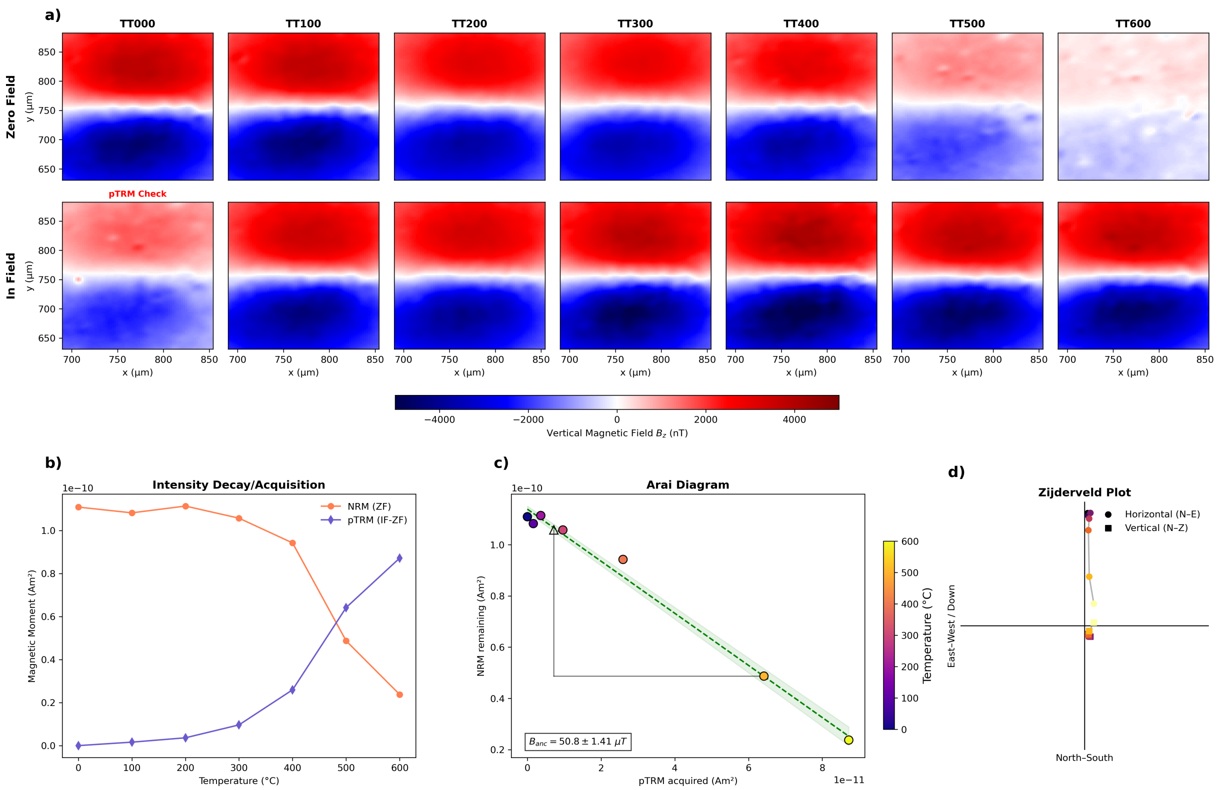

Figure 6: Example of a hand-picked individual magnetic anomaly used for QDM-based Thellier–Thellier paleointensity analysis. (a) Maps of the vertical magnetic field (B_z) measured by QDM at successive thermal steps. The upper row shows the zero-field (ZF) measurements corresponding to the progressive thermal demagnetization of the NRM, while the lower row shows the in-field (IF) measurements used to acquire pTRM at each temperature step. (b) Decay of the NRM (orange) and acquisition of pTRM (blue) derived from the magnetic moment of the selected anomaly. (c) Corresponding Arai diagram with linear regression (green dashed line) used to estimate the paleointensity; the shaded region indicates the uncertainty of the fit. (d) Zijderveld diagram showing the thermal demagnetization behavior of the anomaly, with circles representing the horizontal projection (N–E) and squares the vertical projection (N–Z); colors indicate temperature steps.

materials can also be accessed at https://github.com/compgeolab/micromag-paleoint, where they are distributed under the MIT license for the source code, the CC-BY license for text and figures, and the CC-0 license for the data.

The data analysis was carried out using the Python scientific computing ecosystem. NumPy (Harris et al., 2020) was used for numerical computations and array operations, SciPy (Virtanen et al., 2020) for optimization and linear algebra routines, scikit-image (Van der Walt et al., 2014) for image segmentation and blob detection, Matplotlib (Hunter, 2007) for figure production and stereographic visualizations, Verde (Uieda, 2018) for grid generation and least-squares solutions, Harmonica (Fatiando a Terra Project et al., 2024) for magnetic field processing, upward continuation, and the computation of Schmidt semi-normalized associated Legendre functions and their derivatives, Choclo (Fatiando a Terra Project et al., 2022) for efficient forward-modeling kernel calculations, Numba (Lam et al., 2015) to accelerate computationally intensive routines through just-in-time compilation, and xarray (Hoyer and Hamman, 2017) for managing labeled multidimensional datasets. QDM magnetic field maps were preprocessed using QDMlab (Volk et al., 2022). Fisher directional statistics were calculated using the PmagPy package (Tauxe et al., 2016).

Acknowledgments

We acknowledge the Laboratório de Paleomagnetismo e Magnetismo de Rochas (USPMag, Universidade de São Paulo) for curating the samples and granting access to them. We also thank the Harvard Paleomagnetics Lab (Department of Earth and Planetary Sciences, Harvard University) for making available the facilities and instrumentation used to perform the QDM and bulk measurements. We further recognize the efforts of the developers and maintainers of the open-source software that played a key role in enabling this study. Financial support for this research was provided by Fundação de Amparo à Pesquisa do Estado de São Paulo (FAPESP) through grants 2021/08379-5 and 2023/13372-5 and by Universidade de São Paulo through grant PRPI 22.1.09345.01.2.

References

Bates, H. (2026). Asteroid sample return missions are critical for understanding our solar system. *Nature Communications*, 17(1). doi:10.1038/s41467-026-72265-3.

Bellon, U. D., F. Souza-Junior, G., Williams, W., Muxworthy, A. R., Uieda, L., Fu, R. R., Trindade, R. I. F., and Moraes, C. S. (2026a). Estimating earth's past field strength from individual sources in archaeological ceramics using quantum diamond microscopy. *Communications Earth amp; Environment*. doi:10.1038/s43247-026-03725-3.

Bellon, U. D., Souza-Junior, G. F., Williams, W., Uieda, L., Muxworthy, A. R., Nagy, L., Paterson, G. A., Moraes, C. S., Fu, R., and Trindade, R. I. F. (2026b). Distance-dependent stray field decay in magnetically stable remanence carriers: Implications for magnetic microscopy. *Journal of Geophysical Research: Solid Earth*, 131(3). doi:10.1029/2025jb033133. URL http://dx.doi.org/10.1029/2025JB033133.

Bellon, U. D., Williams, W., Muxworthy, A. R., Souza-Junior, G. F., Nagy, L., Uieda, L., and Trindade, R. I. F. (2025). Efficiency of thermoremanent magnetization acquisition in vortex-state particle assemblies. *Geophysical Research Letters*, 52(8). doi:10.1029/2025gl114771.

Berndt, T., Muxworthy, A. R., and Fabian, K. (2016). Does size matter? Statistical limits of paleomagnetic field reconstruction from small rock specimens. *Journal of Geophysical Research: Solid Earth*, 121(1):15–26. doi:10.1002/2015JB012441.

Bono, R. K., Tarduno, J. A., Nimmo, F., and Cottrell, R. D. (2019). Young inner core inferred from ediacaran ultra-low geomagnetic field intensity. *Nature Geoscience*, 12(2):143–147. doi:10.1038/s41561-018-0288-0.

Bryson, J. F. J., Weiss, B. P., Biersteker, J. B., King, A. J., and Russell, S. S. (2020). Constraints on the distances and timescales of solid migration in the early solar system from meteorite magnetism. *The Astrophysical Journal*, 896(2):103. doi:10.3847/1538-4357/ab91ab. URL http://dx.doi.org/10.3847/1538-4357/ab91ab.

Cai, S., Qin, H., Wang, H., Deng, C., Yang, S., Xu, Y., Zhang, C., Tang, X., Gu, L., Li, X., Shen, Z., Zhang, M., He, K., Qi, K., Fan, Y., Dong, L., Hou, Y., Shi, P., Liu, S., Su, F., Chen, Y., Li, Q., Li, J., Mitchell, R. N., He, H., Li, C., Pan, Y., and Zhu, R. (2025). Persistent but weak magnetic field at the moon's midstage revealed by chang'e-5 basalt. *Science Advances*, 11(1). doi:10.1126/sciadv.adp3333.

Carvallo, C., Roberts, A. P., Leonhardt, R., Laj, C., Kissel, C., Perrin, M., and Camps, P. (2006). Increasing the efficiency of paleointensity analyses by selection of samples using first-order reversal curve diagrams. *Journal of Geophysical Research: Solid Earth*, 111(B12). doi:10.1029/2005jb004126.

Coe, R. S. (1967). Paleo-intensities of the earth's magnetic field determined from tertiary and quaternary rocks. *Journal of Geophysical Research*, 72(12):3247–3262. doi:10.1029/jz072i012p03247. URL http://dx.doi.org/10.1029/JZ072i012p03247.

Dunlop, D. J. and Özdemir, O. (1997). *Rock Magnetism Fundamentals and Frontiers*. Cambridge University Press. doi:10.1017/cbo9780511612794.

Dunlop, D. J., Zhang, B., and Özdemir, O. (2005). Linear and nonlinear thellier paleointensity behavior of natural minerals. *Journal of Geophysical Research: Solid Earth*, 110(B1). doi:10.1029/2004jb003095.

Fatiando a Terra Project, Castro, Y. M., Esteban, F. D., Li, L., Oliveira Jr, V. C., Pesce, A., Shea, N., Soler, S. R., Souza-Junior, G. F., Tankersley, M., Uieda, L., and Uppal, I. (2024). Harmonica v0.7.0: Forward modeling, inversion, and processing gravity and magnetic data [software]. *Zenodo*. doi:10.5281/ZENODO.13308312.

Fatiando a Terra Project, Soler, S. R., and Uieda, L. (2022). Choclo v0.0.1: Kernel functions for your geophysical models [Software]. *Zenodo*. doi:10.5281/zenodo.7851748.

Fisher, N. I., Lewis, T., and Embleton, B. J. J. (1987). *Statistical Analysis of Spherical Data*. Cambridge University Press. ISBN 9780511623059. doi:10.1017/cbo9780511623059.

Fu, R. R., Lima, E. A., Volk, M. W., and Trubko, R. (2020). High-Sensitivity Moment Magnetometry With the Quantum Diamond Microscope. *Geochemistry, Geophysics, Geosystems*, 21(8):e2020GC009147. doi:10.1029/2020GC009147.

Gergov, H., Muxworthy, A. R., Williams, W., and Cowan, A. C. (2025). Magnetic recording fidelity of basalts through 3d nanotomography. *Geochemistry, Geophysics, Geosystems*, 26(3). doi:10.1029/2024gc011776.

Glenn, D. R., Fu, R. R., Kehayias, P., Le Sage, D., Lima, E. A., Weiss, B. P., and Walsworth, R. L. (2017). Micrometer-scale magnetic imaging of geological samples using a quantum diamond microscope. *Geochemistry, Geophysics, Geosystems*, 18(8):3254–3267. doi:10.1002/2017GC006946.

Harris, C. R., Millman, K. J., van der Walt, S. J., Gommers, R., Virtanen, P., Cournapeau, D., Wieser, E., Taylor, J., Bergstra, J., Smith, N. J., Kern, R., Picus, M., Hoyer, S., van Kerkwijk, M. H., Brett, M., Haldane, A., Del Río, J., Wiebe, M., Peterson, P., Gérard-Marchant, P., Sheppard, K., Reddy, T., Weckesser, W., Abbasi, H., Gohlke, C., and Oliphant, T. E. (2020). Array programming with NumPy [software]. *Nature*, 585(7825):357–362. doi:10.1038/s41586-020-2649-2.

Hoyer, S. and Hamman, J. (2017). xarray: N-D labeled arrays and datasets in Python [software]. *Journal of Open Research Software*, 5(1). doi:10.5334/jors.148.

Huang, W., Tarduno, J. A., Zhou, T., Ibañez-Mejia, M., Dal Olmo-Barbosa, L., Koester, E., Blackman, E. G., Smirnov, A. V., Ahrendt, G., Cottrell, R. D., Kodama, K. P., Bono, R. K., Sibeck, D. G., Li, Y.-X., Nimmo, F., Xiao, S., and Watkeys, M. K. (2024). Near-collapse of the geomagnetic field may have contributed to atmospheric oxygenation and animal radiation in the ediacaran period. *Communications Earth amp; Environment*, 5(1). doi:10.1038/s43247-024-01360-4.

Hunter, J. D. (2007). Matplotlib: A 2d graphics environment [software]. *Computing in Science & Engineering*, 9(3):90–95. doi:10.1109/MCSE.2007.55.

Jung, J.-I., Tikoo, S. M., Burns, D., Váci, Z., and Krawczynski, M. J. (2024). Assessing lunar paleointensity variability during the 3.9 - 3.5 ga high field epoch. *Earth and Planetary Science Letters*, 638:118757. doi:10.1016/j.epsl.2024.118757. URL http://dx.doi.org/10.1016/j.epsl.2024.118757.

Kirschvink, J. L. (1980). The least-squares line and plane and the analysis of palaeomagnetic data. *Geophysical Journal International*, 62(3):699–718. doi:10.1111/j.1365-246x.1980.tb02601.x.

Kletetschka, G., Acuna, M., Kohout, T., Wasilewski, P. J., and Connerney, J. E. (2004). An empirical scaling law for acquisition of thermoremanent magnetization. *Earth and Planetary Science Letters*, 226(3–4):521–528. doi:10.1016/j.epsl.2004.08.001.

Lam, S. K., Pitrou, A., and Seibert, S. (2015). Numba: A llvm-based python jit compiler [software]. In *Proceedings of the Second Workshop on the LLVM Compiler Infrastructure in HPC*, pages 1–6.

Levashova, N. M., Golovanova, I. V., Rudko, D., Danukalov, K. N., Rudko, S., Yu, S. R., and Meert, J. G. (2021). Late ediacaran magnetic field hyperactivity: Quantifying the reversal frequency in the zigan formation, southern urals, russia. *Gondwana Research*, 94:133–142. doi:10.1016/j.gr.2021.02.018. URL http://dx.doi.org/10.1016/j.gr.2021.02.018.

Moncinhatto, T. R., Haag, M. B., Hartmann, G. A., Savian, J. F., Poletti, W., Sommer, C. A., Caselli, A. T., and Trindade, R. I. F. (2019). Mineralogical control on the magnetic anisotropy of lavas and ignimbrites: a case study in the caviahue-copahue field (argentina). *Geophysical Journal International*, 220(2):821–838. doi:10.1093/gji/ggz483.

Nagy, L., Williams, W., Tauxe, L., and Muxworthy, A. R. (2019). From nano to micro: Evolution of magnetic domain structures in multidomain magnetite. *Geochemistry, Geophysics, Geosystems*, 20(6):2907–2918. doi:10.1029/2019gc008319. URL http://dx.doi.org/10.1029/2019GC008319.

Néel, L. (1949). Theorie du trainage magnetique des ferromagnetiques en grains fins avec applications aux terres cuites. *Ann. Geophys.*, 5:99–136.

Nichols, C. I. O., Weiss, B. P., Getzin, B. L., Schmitt, H. H., Béguin, A., Rae, A. S. P., and Shah, J. (2021). The palaeoinclination of the ancient lunar magnetic field from an apollo 17 basalt. *Nature Astronomy*, 5(12):1216–1223. doi:10.1038/s41550-021-01469-y. URL http://dx.doi.org/10.1038/s41550-021-01469-y.

Ostermeier, F. K., Gilder, S. A., Wack, M. R., Ježek, J., He, K., and Finn, D. (2026). Determining magnetic field intensity and direction from the anisotropy of magnetic remanence in sediments. *Geochemistry, Geophysics, Geosystems*, 27(4). doi:10.1029/2025gc012676.

Out, F., de Boer, R. A., Walmsley, J., and de Groot, L. V. (2024). The impact of grain-size distributions of iron-oxides on paleomagnetic measurements. *Geochemistry, Geophysics, Geosystems*, 25(4):e2024GC011512. doi:10.1029/2024GC011512.

Poletti, W., Trindade, R. I., Hartmann, G. A., Damiani, N., and Rech, R. M. (2016). Archeomagnetism of jesuit missions in south brazil (1657–1706 ad) and assessment of the south american database. *Earth and Planetary Science Letters*, 445:36–47. doi:10.1016/j.epsl.2016.04.006.

Souza-Junior, G., Uieda, L., Ferreira da Trindade, R., Fu, R., Donardelli Bellon, U., and Moreira Castro, Y. (2025). Robust directional analysis of magnetic microscopy images using non-linear inversion and iterative euler deconvolution. doi:10.31223/x5n42f. URL http://dx.doi.org/10.31223/X5N42F.

Souza-Junior, G. F., Bellon, U. D., de Moraes, C. S., Uieda, L., Fu, R., Williams, W., and Trindade, R. I. F. (2026a). Supplementary material for "On the stability of magnetic paleodirection and paleointensity at microscale" [Dataset]. doi:10.5281/zenodo.21841763.

Souza-Junior, G. F., Bellon, U. D., Uieda, L., Trindade, R. I. F., Fu, R., Williams, W., and Siqueira-Macedo, A. (2026b). Multipole modeling for magnetic microscopy constrained by euler deconvolution. *EarthArXiv*.

Tauxe, L., Shaar, R., Jonestrask, L., Swanson-Hysell, N. L., Minnett, R., Koppers, A. A. P., Constable, C. G., Jarboe, N., Gaastra, K., and Fairchild, L. (2016). Pmagpy: Software package for paleomagnetic data analysis and a bridge to the magnetics information consortium (magic) database [software]. *Geochemistry, Geophysics, Geosystems*, 17(6):2450–2463. doi:10.1002/2016gc006307.

Thellier, E. and Thellier, O. (1959). Sur l'intensité du champ magnétique terrestre dans le passé historique et géologique.

Trindade, R. I. F., Jaqueto, P., Terra-Nova, F., Brandt, D., Hartmann, G. A., Feinberg, J. M., Strauss, B. E., Novello, V. F., Cruz, F. W., Karmann, I., Cheng, H., and Edwards, R. L. (2018). Speleothem record of geomagnetic south atlantic anomaly recurrence. *Proceedings of the National Academy of Sciences*, 115(52):13198–13203. doi:10.1073/pnas.1809197115.

Uieda, L. (2018). Verde: Processing and gridding spatial data using Green's functions [software]. *Journal* *of Open Source Software*, 3(29):957. doi:10.21105/joss.00957.

Van der Walt, S., Schönberger, J. L., Nunez-Iglesias, J., Boulogne, F., Warner, J. D., Yager, N., Gouillart, E., and Yu, T. (2014). scikit-image: image processing in Python [software]. *PeerJ*, 2:e453. doi:10.7717/peerj.453.

Virtanen, P., Gommers, R., Oliphant, T. E., Haberland, M., Reddy, T., Cournapeau, D., Burovski, E., Peterson, P., Weckesser, W., Bright, J., van der Walt, S. J., Brett, M., Wilson, J., Millman, K. J., Mayorov, N., Nelson, A. R. J., Jones, E., Kern, R., Larson, E., Carey, C. J., Polat, I., Feng, Y., Moore, E. W., Vand erPlas, J., Laxalde, D., Perktold, J., Cimrman, R., Henriksen, I., Quintero, E. A., Harris, C. R., Archibald, A. M., Ribeiro, A. H., Pedregosa, F., van Mulbregt, P., and Contributors (2020). SciPy 1.0: Fundamental Algorithms for Scientific Computing in Python [Software]. *Nature Methods*, 17(3):261–272. doi:10.1038/s41592-019-0686-2.

Volk, M. W., Fu, R. R., Trubko, R., Kehayias, P., Glenn, D. R., and Lima, E. A. (2022). Qdmlab: A matlab toolbox for analyzing quantum diamond microscope (qdm) magnetic field maps. *Computers Geosciences*, 167:105198. doi:https://doi.org/10.1016/j.cageo.2022.105198.

Weiss, B. P., Lima, E. A., Fong, L. E., and Baudenbacher, F. J. (2007). Paleomagnetic analysis using SQUID microscopy. *Journal of Geophysical Research: Solid Earth*, 112(9):9105. doi:10.1029/2007JB004940.

Weiss, B. P., Mansbach, E. N., Maurel, C., Sprain, C. J., Swanson-Hysell, N. L., and Williams, W. (2025). What we can learn about mars from the magnetism of returned samples. *Proceedings of the National Academy of Sciences*, 122(2). doi:10.1073/pnas.2404259121.